THE JOURNAL OF PHYSICAL CHEMISTRY Letters

pubs.acs.org/JPCL Letter

Single-Protein Collapse Determines Phase Equilibria of a Biological Condensate

Han-Yi Chou and Aleksei Aksimentiev*

Cite This: J. Phys. Chem. Lett. 2020, 11, 4923−4929 Read Online

ACCESS | Metrics & More | Article Recommendations | Supporting Information

ABSTRACT: Recent advances in microscopy of living cells have established membraneless organelles as critical elements of diverse biological processes. The body of experimental work suggests that formation of such organelles is driven by liquid−liquid phase separation, a physical process that has been studied extensively for both simple liquids and mixtures of polymers. Here, we combine molecular dynamics simulations with polymer theory to show that the thermodynamic behavior of one particular biomolecular condensate—fused in sarcoma (FUS)—can be quantitatively accounted for at the level of the chain collapse theory. First, we show that a particle-based molecular dynamics model can reproduce known phase separation properties of a FUS condensate, including its critical concentration and susceptibility to mutations. Next, we obtain a polymer physics representation of a FUS condensate by examining the behavior of a single FUS protein as a function of temperature. We use the chain collapse theory to determine the thermodynamic properties of the condensate and to characterize changes in the single-chain conformation at the onset of phase separation. Altogether, our findings suggest that the phase behavior of FUS condensates can be explained by the properties of individual FUS proteins and that the change in the FUS conformation is the main force driving for the phase separation.

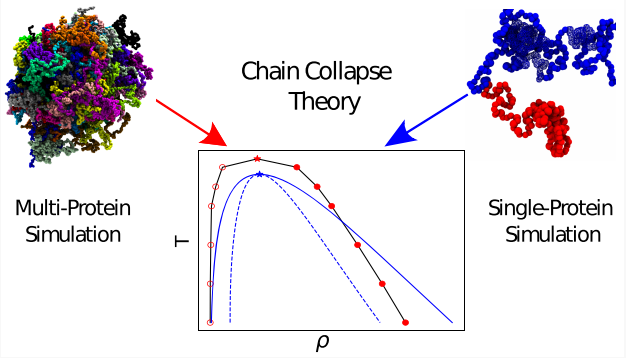

Biological cells have long been known to use membrane-enclosed organelles to isolate biochemical processes, increasing their efficiency and limiting the effects of toxic intermediates.[1] Organelles lacking such membranes, i.e., granules and inclusion bodies, were thought to be passive agglomerations of spare biomolecular parts with no known purpose beyond serving as a cellular pantry. Recent experimental work,[2,3] however, suggests that such membraneless organelles are in fact liquid-like biomolecular condensates that precipitate from cellular cytosol or nucleoplasm in response to specific biochemical signals and provide an organelle-like environment for biochemical processes without needing to confine them using a physical barrier.[4−8] Although we do not yet know the molecular mechanisms governing formation of these biological condensates, we know that they play central roles in the processes of DNA repair and gene regulation,[9] growth of a multicellular organism,[10] and many neurodegenerative diseases such as amyotrophic lateral sclerosis.[11,12]

Here, we combine coarse-grained (CG) molecular dynamics simulations with a polymer theory to show that the phase behavior of a biological condensate can be deduced by studying the behavior of isolated proteins comprising the condensate. As a subject of our study, we chose the fused in sarcoma (FUS) protein,[12−14] which experiment has identified as the principal component of a biological condensate involved in DNA repair.[13] A FUS protein contains 526 amino acids that form several structured and disordered domains (Figure 1a). The structure of FUS can be broadly divided into the following two parts: the intrinsically disordered prion-like domain (PLD), residue 1-163, that contains only a few types of amino acids such as glycine, glutamine, serine, and tyrosine and the RNA-binding domain (RBD), residue 164-526, which contains both intrinsically disordered and structured regions, the most notable structured region being an RNA recognition motif. It is believed that the intrinsically disordered PLD of FUS is the main component enabling the liquid−liquid phase separation (LLPS). Several CG molecular dynamics (MD) studies examined the phase behavior of PLD,[15,16] whereas field-theory approaches[17,18] and lattice models[19−21] were applied to examine the phase behavior of related intrinsically disordered proteins. Recent experimental study have identified the interactions between the arginine residues of RBD and the tyrosine residues of PLDs as the principal determinant of FUS's phase separation behavior: mutating either one prevented formation of the condensates at

Received: April 21, 2020
Accepted: May 19, 2020
Published: May 19, 2020

https://dx.doi.org/10.1021/acs.jpclett.0c01222
J. Phys. Chem. Lett. 2020, 11, 4923−4929

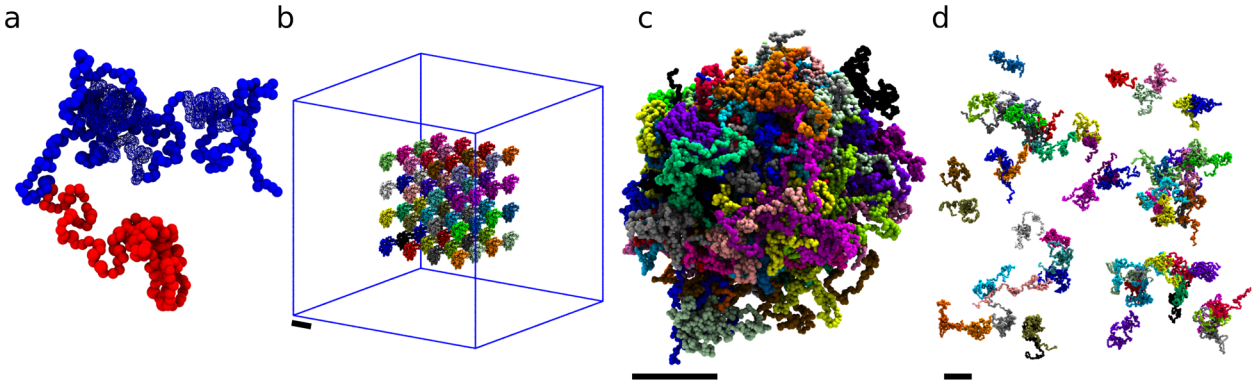

Figure 1. Coarse-grained molecular dynamics simulation of FUS condensation. (a) The computational model of FUS where each bead represents one amino acid of the protein. The beads comprising the PLD domain are shown in red, whereas those of RBD are shown in blue. The wireframe surface represents the structured domains of FUS, residues 278−385 (EP1 domain), and 419−454 (GP1 domain). (b) Initial configuration of the simulation system where 64 copies of the FUS protein are arranged on a 4×4 lattice. The simulation box measures $91 \times 91 \times 91$ nm^3. Each protein copy is shown using a different color. (c) Final configuration of the wild-type (WT) FUS system obtained at the end of a ∼1 μs simulation at 292 K. (d) Final configuration of the R → K mutant FUS system obtained from a simulation that was performed under conditions identical to those as for the WT FUS, panel c. Replacing arginines with lysine residues in WT FUS was experimentally found to prevent FUS condensation.[13] The scale bars in panels b−d correspond to 10 nm.

biologically accessible concentrations of FUS.[13] The molecular mechanism giving rise to such phenomenological observations, however, remains elusive.

We constructed our CG model of a FUS protein by representing each amino acid residue of the protein by one CG bead (Figure 1a). The bonded interactions within the protein were described by harmonic spring potentials (10 kJ/(mol Å^2) spring constant and 3.8 Å equilibrium length) that connected the neighboring residues of the protein chain.[15] The nonbonded interaction between the residues were described using the Kim−Hummer (KH) model,[22] accounting for the difference in the KH parameters describing the structured and disordered parts of the proteins.[15] In accordance with the KH model, the electrostatic interaction between the charged residues was described within the Debye−Hückel approximation with a temperature-dependent screening length that varied between 7.8 and 10.2 Å. The 3D shape of the structured domains was maintained using harmonic distance restraints applied to pairs of residues located within 12 and 8 Å of each other for the EP1 and GP1 domains, respectively.

We used our CG model to recapitulate key experimental observations regarding the phase behavior of the condensate. In a typical simulation, 64 copies of the FUS protein were arranged on a lattice and placed within a cubic simulation cell (Figure 1b), corresponding to the overall FUS concentration of 0.14 mM. The system was simulated using the Langevin dynamics with a time step of 10 fs, the damping coefficient of 0.01 ps^{-1}, and at 292 K using the LAMMPS software package (19 Sep 2019 version).[23] After ∼1 μs simulation, 64 wild-type (WT) FUS proteins were observed to condense into one liquid-like droplet of the average FUS concentration of 7.8 mM (Figure 1c and Supporting Movie 1). Such spontaneous condensation is a hallmark of phase separation, where an initially homogeneous system, upon quench of external conditions,[8,24,25] spontaneously develops two phases, one being the condensed phase (the droplet in our case) and the other being the dispersed phase, which, in our case, is the volume outside the droplet containing no FUS. To test the chemical specificity of our model, we repeated our simulation using a mutant version of the FUS protein where all 37 arginine residues of the RBD domain were replaced by lysine residues. The protein configuration obtained after ∼1 μs (Figure 1d and Supporting Movie 2) shows little resemblance to the phase separation behavior seen for the WT FUS system (Figure 1c). Similar abolishment of phase separation behavior was previously observed in experiment.[13] Given that both arginine and lysine residues carry the same positive charge, the qualitatively different outcome of the simulations observed upon subtle mutation indicates that our CG model of FUS is capable of capturing the essential features of the corresponding experimental system.

While clearly showing a phase separation behavior, the simulations above are ill-suited for quantitative analysis of phase equilibria because such analysis requires accurate determination of FUS concentration in the dispersed phase, a concentration that could be 1000 times smaller than that of the condensed phase. We characterized the phase equilibria of the WT FUS system using the so-called slab method,[26−28] which was originally developed to study the coexistence of liquid and gas phases in Lennard-Jones fluids and has been adopted to study the LLPS behavior.[15] First, a system containing 125 FUS proteins in a $40 \times 40 \times 40$ nm^3 volume was quenched to 150 K in a 200 ns simulation carried out in the isotropic constant number of particles, pressure, and temperature (*NPT*) ensemble. Following that, the simulation system was enlarged 20 times along the *z*-axis, which was followed by a collection of production runs carried out in the constant number of particles, volume, and temperature (*NVT*) ensemble. In each run, the temperature was gradually increased to the target temperature at a rate of 0.9 K/ns following which each system was simulated for 3 μs; the first 1 μs of each trajectory was discarded from the analysis. These simulations employed a 20 fs time step and the Nóse−Hoover style non-Hamiltonian equations of motion for both *NPT* and *NVT* ensembles.

Figure 2a and Supporting Movie 3 show representative configurations from the slab simulations at three different temperatures. As the temperature increases, the dispersed phase emerges. At 340 K, the entire simulation system consists of a dispersed phase, suggesting that this simulation was performed above the critical temperature. To systematically determine the critical temperature, the critical density, and the phase diagram, we determined the density profile of FUS along the *z*-axis as a function of temperature (Figure 2b). The density profiles

https://dx.doi.org/10.1021/acs.jpclett.0c01222
J. Phys. Chem. Lett. 2020, 11, 4923−4929

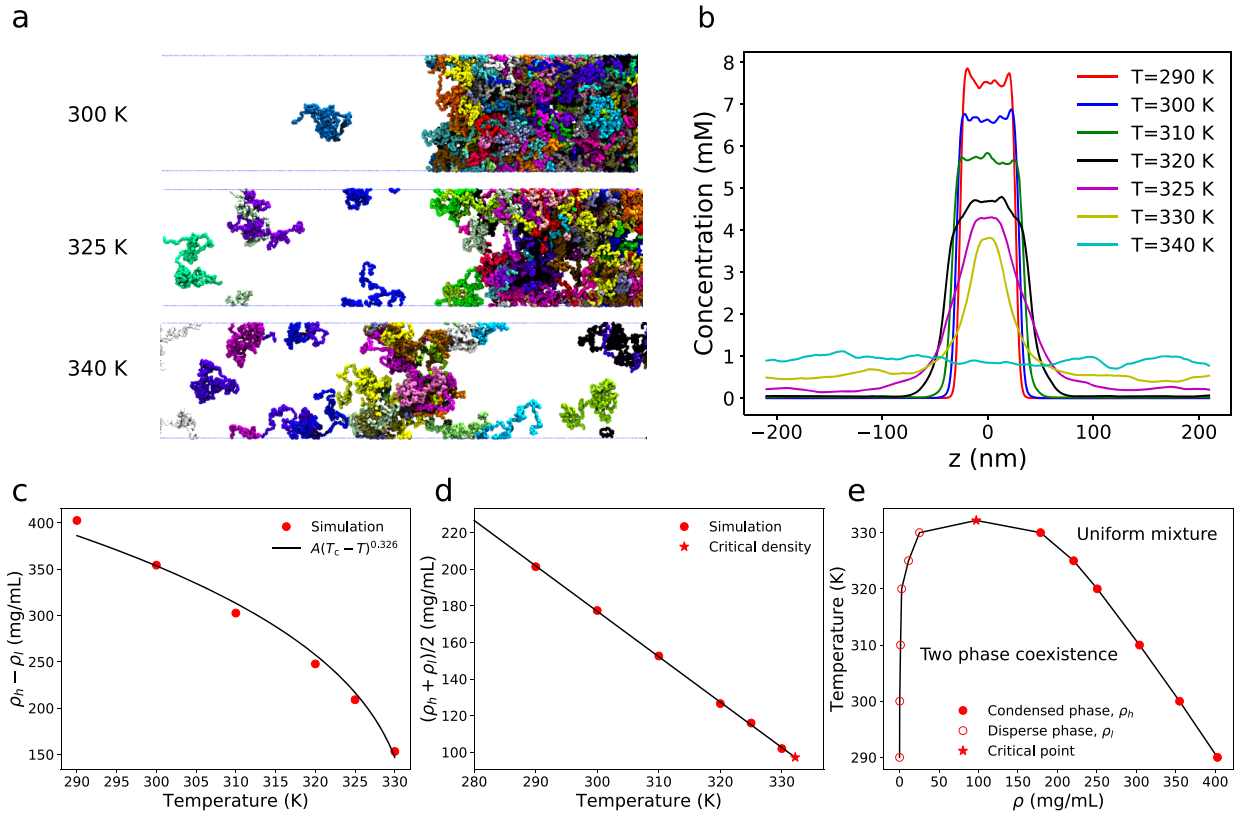

Figure 2. Slab method calculation of phase equilibria. (a) Representative configuration of the simulation system at three different temperatures. (b) Profile of FUS density along the z-axis. The density profile was computed by first aligning each frame of the simulation trajectory to have the center of mass of the largest cluster located at $z = 0$. A cluster was defined as a collection of molecules where any molecule was within 35 Å of another molecule from the same cluster along the z-axis. For reference, the average radius of gyration of a FUS molecule in the condensed phase is 57 Å. (c) Density difference between the condensed, ρ_h, and dispersed, ρ_l, phases versus temperature (red circles). The average concentration of FUS in the phases was computed by averaging the $|z| < 20$ nm and $|z| > 150$ nm regions of the concentration profiles, respectively, shown in panel b. The solid line shows a power law fit, $A(T - T_c)^{\beta}$, with the critical exponent of the 3D Ising model, $\beta = 0.326$. (d) The law of rectilinear diameters fit to the data. A star symbol shows the critical density, $\rho_c = 97$ mg/mL. (e) Binodal curve of a FUS condensate obtained directly from MD simulations. Empty/filled circles indicate the density of the dispersed/condensed phases at a specified temperature. The critical point is marked by a star symbol.

indicate that the critical temperature lies between 330 and 340 K. Knowing the density of each phase, we defined the density difference as the order parameter. Following the Landau theory for the continuous second-order phase transition,[29] we estimated the critical temperature by fitting the order parameter to the power law $A(T - T_c)^{\beta}$ with the critical exponent $\beta = 0.326$, which assumes that the phase transition belongs to the 3D Ising universality class.[30] The critical temperature, T_c, extracted from the fit was 332.2 K. The critical density was estimated by assuming the law of rectilinear diameters,[31] $\rho = \rho_c + B(T_c - T)$, which yielded the critical density of 97 mg/mL (Figure 2d). Using the density of the coexisting phases at different temperatures, we charted an approximate phase diagram of a WT FUS condensate (Figure 2e). According to our phase diagram, the FUS concentration in the dispersed phase at 300 K is 4.7 μM, which is in close agreement with experiment[13,32] that found the FUS system develops a two-phase behavior at FUS concentrations exceeding 5 μM.

From a thermodynamics point of view, the LLPS behavior emerges as a competition of the intra- and intermolecular interactions and the entropy of the FUS chain configurations.[33] Polymers that exhibit stronger attraction between monomers tend to have smaller radius of gyration (R_g) under poor solvent conditions and, intuitively, can be expected to form more dense condensates and require higher temperature to dissolve. Zeng et al. have recently shown[34,35] how the theory single chain collapse theory of Raos and Allegra[36] can be used to extract relevant parameters from profiles of single chain coil-globule transitions in order to compute full phase diagrams. We use their approach to test if the phase behavior of a biological condensate, with all the complexity of its inter- and intramolecular interactions, can indeed be described by a rather simple polymer physics model.

In the chain collapse theory, an individual polymer chain consisting of N Kuhn segments of length l is described at the level of the mean-field theory.[36] To map the full-length FUS protein to such a representation, each of its structured domains was first replaced by a virtual CG bead located at the center of mass of the domain and having the same mass as the domain. Thus, our polymer chain model of FUS contained only 384 monomers that represented 526 residues.

The number of Kuhn segments, N, of length l that represent a CG polymer of $N_0 + 1$ beads and the interbead length l_0 can be determined from

$$Nl = N_0 l_0 \sin\left(\frac{\psi}{2}\right) \quad (1)$$

$$\langle R_g^2 \rangle_\theta = \frac{1}{6} Nl^2 \quad (2)$$

https://dx.doi.org/10.1021/acs.jpclett.0c01222
J. Phys. Chem. Lett. 2020, 11, 4923−4929

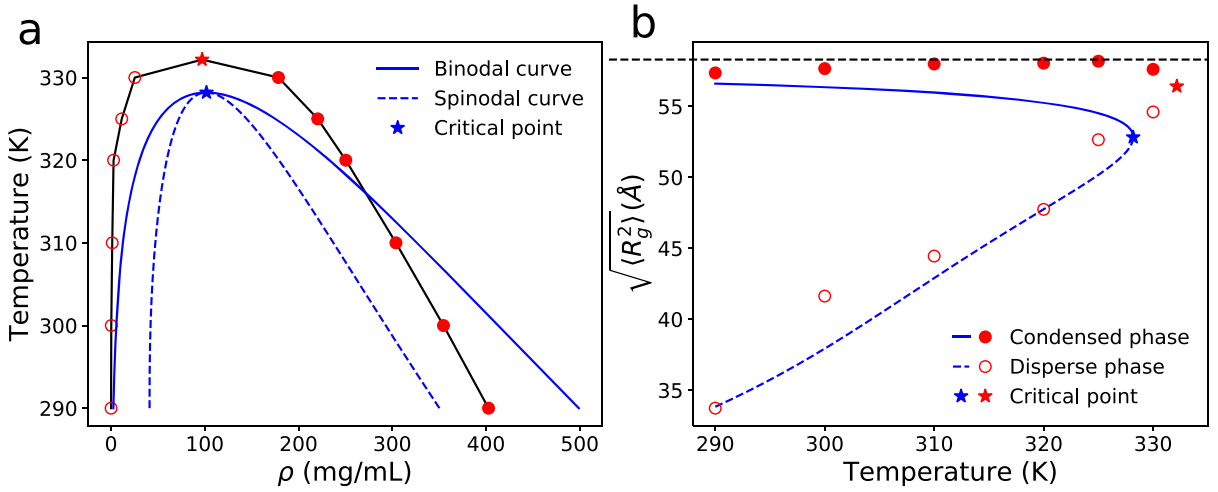

Figure 3. Chain collapse theory description of FUS phase behavior. (a) Phase equilibria of FUS according to the single-chain collapse theory (blue line). Data from MD simulations (same as in Figure 2e) are plotted in red for comparison. (b) Mean squared radius of gyration of FUS as a function of temperature. Data from the chain collapse theory and MD simulations are shown in blue and red, respectively. The MD values of $\sqrt{\langle R_g^2 \rangle}$ were obtained by averaging over $|z| < 20$ nm and $|z| > 150$ nm regions of the simulation system after alignment, see Figure 2b. The MD data for the critical point were obtained by analyzing the last 2 μs of a 3 μs trajectory of 24 FUS proteins simulated at the critical temperature of 328.2 K and the critical density of 102 mg/mL. For reference, the black dashed line indicates the $\sqrt{\langle R_g^2 \rangle}$ value of a single FUS protein at θ temperature.

where l_0 and ψ are the average distance between the consecutive beads and the average angle between the two consecutive bonds, respectively, of a FUS polymer and $\langle R_g^2 \rangle_\theta$ is the polymer's average radius of gyration at θ temperature.

To carry out such mapping, we first determined the θ temperature (T_θ) of the FUS protein by simulating individual proteins for 5 μs at several temperatures maintained using a Nöse−Hoover thermostat. After discarding the first 2 μs, we determined the scaling exponent (ν) that best describes the asymptotic relation $\langle R_g(|i-j|) \rangle \sim |i-j|^\nu$ as the difference of the polymer bead indices $|i-j| \to \infty$ (Supporting Figure S1a). At T_θ, the scaling exponent ν equals that of a random walk, i.e., 0.5, which for FUS we found to be at 400 K (Supporting Figure S1b).

We then used a single-chain simulation at 290 K to extract the average bond length $l_0 = 4.13$ Å and the average bond angle $\psi = 115.2°$ and verified that those quantities depend very weakly on temperature (Supporting Figure S2).

At a given temperature, the free energy of a single polymer chain (in units of k_BT) is[36]

$$\mathcal{A}(q;\tau) = \tau B\sqrt{N}2^{-5/2}\sigma^{-3} + \frac{k\sigma^{-6}}{2\times 3^{5/2}} + \frac{3}{2}\left[\ln\left(\frac{\sinh q}{q}\right) - \frac{1}{2}q\left(\coth q - \frac{1}{q}\right)\right] \quad (3)$$

$$\langle \sigma^2 \rangle \equiv \frac{\langle R_g^2 \rangle}{Nl^2} = \frac{1}{2q}\left(\coth q - \frac{1}{2q}\right) \quad (4)$$

where $\tau \equiv (T - T_\theta)/T$ denotes the reduced temperature, τB and K are the second and the third virial coefficients of the Kuhn segment, and σ^2 denotes the ratio of the polymer's average radius of gyration at that temperature to the square of the polymer's end-to-end distance at the θ temperature. The first two terms in eq 3 correspond to the two- and three-body interaction between the monomers whereas the last term describes the entropic contribution. Equation 4 prescribes a one-to-one relationship between σ^2 and a monotonically decreasing function of parameter q, which was introduced to obtain the analytical expressions for the free energy, albeit in a parametric form.

We found the numerical values of parameters B and K from the conditions of thermal equilibrium,[36] $\frac{d\mathcal{A}(q;\tau)}{dq} = 0$, i.e.

$$-\tau NB - \left(\frac{2}{3}\right)^{5/2} \times \frac{k}{\sigma^3} = 2^{7/2}\sigma^5\left[\frac{\coth q}{2} + \frac{q}{2\sinh^2 q} - \frac{1}{q}\right]\left[\frac{1}{q\sinh^2 q} + \frac{\coth q}{q^2} - \frac{2}{q^3}\right]^{-1} \quad (5)$$

which must be satisfied at any temperature, τ. Using the previously determined dependence of $\langle R_g^2 \rangle$ on temperature (Supporting Figure S1a) and the polymer end-to-end distance at θ temperature, 142.8 Å, we determined the values of σ and, through eq 4, of q at several temperatures (Supporting Figure S3). Entering these σ^2 and q values into eq 5 produced a set of linear equitations, which was solved for B and K using the least-squares fit method. The results of the fitting procedure are shown in Supporting Figure S3.

According to ref 36, the free energy of a single chain inside an infinite cluster of chains (in units of k_BT) is

$$\mathcal{F}(q,\phi;\tau) = (\tau B + kF\phi)\sqrt{N}2^{-5/2}\sigma^{-3} + \frac{k\sigma^{-6}}{2\times 3^{5/2}} + \frac{1}{2}\tau BNF\phi + 4\times 3^{-5/2}kN(F\phi)^2 + \log\left(\frac{E\phi}{N}\right) + \frac{3}{2}\left[\log\left(\frac{\sinh q}{q}\right) - \frac{q}{2}\left(\coth q - \frac{1}{q}\right)\right] + \left[\frac{3}{2}\log\left(\frac{3}{\pi} - \frac{5}{2}\right)\right] \quad (6)$$

where ϕ is the polymer volume fraction and the numerical values of the constants $E = \frac{DNl_0^3}{2^{3/2}N_0v_c}$ and $F = E\left(\frac{l}{l_0}\right)^3$ are determined by

https://dx.doi.org/10.1021/acs.jpclett.0c01222
J. Phys. Chem. Lett. 2020, 11, 4923−4929

the two system-dependent parameters, D and v_c. Here, D specifies the ratio of the cluster's pervaded volume to the cube of the radius of gyration of the cluster, which we chose to be 8, corresponding to a cubic approximation for the shape of the chains. The v_c parameter[36] defines the effective volume of the chain's monomer and is in turn related to the bond length l_0, the three-body interaction strength k, and C_∞ as $v_c = l_0^3\sqrt{k}\left(\frac{2}{3}\pi c_\infty\right)$, where $C_\infty = \frac{Nl^2}{N_0 l_0^2}$.

With eq 6 at hand, we can obtain the binodal and spinodal curves numerically[36] (Figure 3a). The binodal curve was obtained by equating the chemical potential (μ) and the osmotic pressure (π) of the two phases and imposing the variational condition on the cluster free energy at any given ϕ:

$$\mu|_{\phi=\phi_h,q=q_h} = \mu|_{\phi=\phi_l,q=q_l} \tag{7}$$

$$\pi|_{\phi=\phi_h,q=q_h} = \pi|_{\phi=\phi_l,q=q_l} \tag{8}$$

$$\left(\frac{\partial \mathcal{F}}{\partial q}\right)_\phi|_{\phi=\phi_h,q=q_h} = \left(\frac{\partial \mathcal{F}}{\partial q}\right)_\phi|_{\phi=\phi_l,q=q_l} = 0 \tag{9}$$

where ϕ_h and ϕ_l denote the polymer volume fraction at the condensed and dispersed phase, respectively, with the corresponding q_h and q_l values. In the above, the chemical potential[36] is

$$\mu = \mathcal{F} + \phi\frac{\partial \mathcal{F}}{\partial \phi} \tag{10}$$

whereas the osmotic pressure is

$$\frac{\pi}{k_B T} = \frac{\phi^2}{N_0 v_c}\frac{\partial \mathcal{F}}{\partial \phi} \tag{11}$$

The spinodal curve was obtained by solving

$$\frac{\partial^2(\phi\mathcal{F})}{\partial \phi^2}|_{\phi=\phi_h',q=q_h'} = \frac{\partial^2(\phi\mathcal{F})}{\partial \phi^2}|_{\phi=\phi_l',q=q_l'} = 0 \tag{12}$$

$$\left(\frac{\partial \mathcal{F}}{\partial q}\right)_\phi|_{\phi=\phi_h',q=q_h'} = \left(\frac{\partial \mathcal{F}}{\partial q}\right)_\phi|_{\phi=\phi_l',q=q_l'} = 0 \tag{13}$$

and in addition to eqs 12 and 13, the critical point satisfies

$$\frac{\partial^3}{\partial \phi^3}[\phi\mathcal{F}(q, \phi; \tau)]|_{\phi=\phi_c,q=q_c} = 0 \tag{14}$$

where ϕ' and ϕ_c represent the states at the spinodal curve and the critical point, respectively.

To compare directly the predictions of the chain collapse theory to the MD data, we converted the polymer volume fraction ϕ to the polymer density ρ using $\rho = M\phi/(N_0 v_c)$, where M is the total mass of the chain. Figure 3a shows that the binodal curve obtained from the chain collapse theory matches quantitatively the binodal curve extracted from our MD simulations. Furthermore, the critical temperature and the critical density obtained by solving eq 14 numerically, 328.2 K and 102 mg/mL, respectively, are also in good agreement with the values obtained from the MD simulations, 332.2 K and 97 mg/mL.

To gain more insight into the microscopic phenomena that give raise to the phase diagram, we computed the mean squared radius of gyration of individual FUS proteins in the condensed and dispersed phases along the binodal curve directly from our MD simulations and using the chain collapse theory (Figure 3b). The latter was accomplished by converting q to $\sqrt{\langle R_g^2\rangle}$ through eq 4. Direct analysis of our MD trajectories and the chain collapse theory both show that the conformations of individual FUS molecules are much more extended in the condensed phase than in the dispersed phase. As the temperature increases, $\langle R_g^2\rangle$ increases prominently in the dispersed phase but changes only by a small amount in the condensed phase.

The above behavior could be explained as follows: The chain inside a cluster adopts a more extended conformation than in isolation because, under poor solvent conditions,[37,38] an extended conformation both lowers the interchain interaction energy and increases the chain's entropy. When the temperature increases, an isolated chain in the dispersed phase expands to maximize its entropy. In the condensed phase, however, the chains's conformation is already close to that at the θ temperature (Figure 3b), which leaves little room for changing the conformation further. The chain collapse theory, however, predicts a modest decrease of $\langle R_g^2\rangle$ in the condensed phase as the system approaches the critical point, a trend that has also been seen in CG MD simulations of polymers near the θ temperature.[39] The chain size increase in the dispersed phase meets the slight chain size decrease in the condensed phase at the critical point, where the two phases have the same chain conformations. Conversely, when a uniform system is quenched from the θ temperature, the interchain distance shrinks, driving the formation of the condensed phase whereas a single-chain collapse drives the formation of the dispersed phase.

Looking at the critical point as a conformational transition, one can explain the results of the previous studies[15,40] that found the θ temperature of a protein to be positively correlated with the critical temperature of the LLPS and with the R_g of the protein. At $T = T_\theta$, the molecules of the condensate behave as ideal chains of noninteracting monomers, a physical situation that excludes chain collapse and thus LLPS. As the temperature increases, the phase separation should disappear at $T = T_\theta$, at the latest. Thus, T_θ sets the upper bound for the critical temperature value, and the higher the upper-bound, the more likely it is for the critical temperature to have a higher value.

In conclusion, we have used MD simulations and the chain collapse theory to chart the phase diagram of a biological condensate formed by FUS proteins. Apart from some minor discrepancies near the critical point, where concentration fluctuations can be expected to be strong,[41,42] we found the chain collapse theory to quantitatively describe the thermodynamical properties of the FUS condensate observed directly in MD simulations, which suggests that collapse of a single-protein conformation is the primary driver of the phase separation. From a practical point of view, our study provides a computationally efficient strategy for the evaluation of the phase diagram that can also be applied to all-atom explicit solvent models of biocondensate molecules. Our work sets the stage for future studies that will elucidate the molecular mechanisms driving LLPS in complex biological condensates that contain two or more biomolecular species, including the highly charged RNA, which can be expected to significantly enrich phase behavior.[43]

https://dx.doi.org/10.1021/acs.jpclett.0c01222
J. Phys. Chem. Lett. 2020, 11, 4923−4929

■ ASSOCIATED CONTENT

Supporting Information

The Supporting Information is available free of charge at https://pubs.acs.org/doi/10.1021/acs.jpclett.0c01222.

Plots detailing the results of CG MD simulations of single FUS proteins used for parametrization of the chain collapse model (PDF)

Supporting Movie 1: Animation illustrating a CG MD simulation of 64 WT FUS proteins at 292 K, forming a liquid-like droplet after ∼1 μs (MP4)

Supporting Movie 2: Animation illustrating a CG MD simulation of 64 (R → K) FUS mutants at 292 K, remaining dispersed state after ∼1 μs (MP4)

Supporting Movie 3: Animation illustrating three CG MD simulations of a slab FUS system performed at different temperatures (MP4)

■ AUTHOR INFORMATION

Corresponding Author

Aleksei Aksimentiev − *Department of Physics, University of Illinois at Urbana−Champaign, Urbana, Illinois 61801, United States;* orcid.org/0000-0002-6042-8442; Email: aksiment@illinois.edu

Author

Han-Yi Chou − *Department of Physics, University of Illinois at Urbana−Champaign, Urbana, Illinois 61801, United States*

Complete contact information is available at: https://pubs.acs.org/10.1021/acs.jpclett.0c01222

Notes

The authors declare no competing financial interest.

■ ACKNOWLEDGMENTS

This work was supported via grants from the National Science Foundation (PHY-1430124, DMR-1827346) and the National Institutes of Health (P41-GM104601). Computer time was provided by the Leadership Resource Allocation MCB20012 on Frontera at Texas Advanced Computing Center. We are grateful to Dr. Xiangze Zeng from the Pappu lab at Washington University in St. Louis for sharing unpublished results with us, guiding us through our usage of the theory of Raos and Allegra, and for fostering transparency in scientific communication.

■ REFERENCES

(1) Gennis, R. B. *Biomembranes: Molecular Structure and Function*; Springer-Verlag: New York, 1989.

(2) Burke, K. A.; Janke, A. M.; Rhine, C. L.; Fawzi, N. L. Residue-by-Residue View of *in vitro* FUS Granules that Bind the C-Terminal Domain of RNA Polymerase II. *Mol. Cell* **2015**, *60*, 231−241.

(3) Guo, L.; Shorter, J. It's Raining Liquids: RNA Tunes Viscoelasticity and Dynamics of Membraneless Organelles. *Mol. Cell* **2015**, *60*, 189−192.

(4) Banani, S. F.; Lee, H. O.; Hyman, A. A.; Rosen, M. K. Biomolecular Condensates: Organizers of Cellular Biochemistry. *Nat. Rev. Mol. Cell Biol.* **2017**, *18*, 285−298.

(5) Shin, Y.; Brangwynne, C. P. Liquid Phase Condensation in Cell Physiology and Disease. *Science* **2017**, *357*, No. eaaf4382.

(6) Brangwynne, C. P.; Eckmann, C. R.; Courson, D. S.; Rybarska, A.; Hoege, C.; Gharakhani, J.; Jülicher, F.; Hyman, A. A. Germline P Granules are Liquid Droplets that Localize by Controlled Dissolution/Condensation. *Science* **2009**, *324*, 1729−1732.

(7) Feric, M.; Vaidya, N.; Harmon, T. S.; Mitrea, D. M.; Zhu, L.; Richardson, T. M.; Kriwacki, R. W.; Pappu, R. V.; Brangwynne, C. P. Coexisting Liquid Phases Underlie Nucleolar Subcompartments. *Cell* **2016**, *165*, 1686−1697.

(8) Hyman, A. A.; Weber, C. A.; Jülicher, F. Liquid−Liquid Phase Separation in Biology. *Annu. Rev. Cell Dev. Biol.* **2014**, *30*, 39−58.

(9) Naumann, M.; Pal, A.; Goswami, A.; Lojewski, X.; Japtok, J.; Vehlow, A.; Naujock, M.; Günther, R.; Jin, M.; Stanslowsky, N.; et al. Impaired DNA Damage Response Signaling by FUS-NLS Mutations Leads to Neurodegeneration and FUS Aggregate Formation. *Nat. Commun.* **2018**, *9*, 335.

(10) Quiroz, F. G.; Fiore, V. F.; Levorse, J.; Polak, L.; Wong, E.; Pasolli, H. A.; Fuchs, E. Liquid−Liquid Phase Separation Drives Skin Barrier Formation. *Science* **2020**, *367*, eaax9554.

(11) Kwiatkowski, T. J.; Bosco, D. A.; LeClerc, A. L.; Tamrazian, E.; Vanderburg, C. R.; Russ, C.; Davis, A.; Gilchrist, J.; Kasarskis, E. J.; Munsat, T.; et al. Mutations in the FUS/TLS Gene on Chromosome 16 Cause Familial Amyotrophic Lateral Sclerosis. *Science* **2009**, *323*, 1205−1208.

(12) Vance, C.; Rogelj, B.; Hortobágyi, T.; De Vos, K. J.; Nishimura, A. L.; Sreedharan, J.; Hu, X.; Smith, B.; Ruddy, D.; Wright, P.; et al. Mutations in FUS, an RNA Processing Protein, Cause Familial Amyotrophic Lateral Sclerosis Type 6. *Science* **2009**, *323*, 1208−1211.

(13) Wang, J.; Choi, J.-M.; Holehouse, A. S.; Lee, H. O.; Zhang, X.; Jahnel, M.; Maharana, S.; Lemaitre, R.; Pozniakovsky, A.; Drechsel, D.; et al. A Molecular Grammar Governing the Driving Forces for Phase Separation of Prion-Like RNA Binding Proteins. *Cell* **2018**, *174*, 688−699.

(14) Niaki, A. G.; Sarkar, J.; Cai, X.; Rhine, K.; Vidaurre, V.; Guy, B.; Hurst, M.; Lee, J. C.; Koh, H. R.; Guo, L.; et al. Loss of Dynamic RNA Interaction and Aberrant Phase Separation Induced by Two Distinct Types of ALS/FTD-Linked FUS Mutations. *Mol. Cell* **2020**, *77*, 82−94.

(15) Dignon, G. L.; Zheng, W.; Kim, Y. C.; Best, R. B.; Mittal, J. Sequence Determinants of Protein Phase Behavior from a Coarse-Grained Model. *PLoS Comput. Biol.* **2018**, *14*, e1005941.

(16) Dignon, G. L.; Zheng, W.; Best, R. B.; Kim, Y. C.; Mittal, J. Relation Between Single-Molecule Properties and Phase Behavior of Intrinsically Disordered Proteins. *Proc. Natl. Acad. Sci. U. S. A.* **2018**, *115*, 9929−9934.

(17) Lin, Y.-H.; Forman-Kay, J. D.; Chan, H. S. Sequence-Specific Polyampholyte Phase Separation in Membraneless Organelles. *Phys. Rev. Lett.* **2016**, *117*, 178101.

(18) McCarty, J.; Delaney, K. T.; Danielsen, S. P. O.; Fredrickson, G. H.; Shea, J.-E. Complete Phase Diagram for Liquid−Liquid Phase Separation of Intrinsically Disordered Proteins. *J. Phys. Chem. Lett.* **2019**, *10*, 1644−1652.

(19) Das, S.; Eisen, A.; Lin, Y.-H.; Chan, H. S. A Lattice Model of Charge-Pattern-Dependent Polyampholyte Phase Separation. *J. Phys. Chem. B* **2018**, *122*, 5418−5431.

(20) Choi, J.-M.; Dar, F.; Pappu, R. V. LASSI: A Lattice Model for Simulating Phase Transitions of Multivalent Proteins. *PLoS Comput. Biol.* **2019**, *15*, e1007028.

(21) Martin, E. W.; Holehouse, A. S.; Peran, I.; Farag, M.; Incicco, J. J.; Bremer, A.; Grace, C. R.; Soranno, A.; Pappu, R. V.; Mittag, T. Valence and Patterning of Aromatic Residues Determine the Phase Behavior of Prion-Like Domains. *Science* **2020**, *367*, 694−699.

(22) Kim, Y. C.; Hummer, G. Coarse-Grained Models for Simulations of Multiprotein Complexes: Application to Ubiquitin Binding. *J. Mol. Biol.* **2008**, *375*, 1416−1433.

(23) Plimpton, S. Fast Parallel Algorithms for Short-Range Molecular Dynamics. *J. Comput. Phys.* **1995**, *117*, 1−19.

(24) Falahati, H.; Haji-Akbari, A. Thermodynamically Driven Assemblies and Liquid−Liquid Phase Separations in Biology. *Soft Matter* **2019**, *15*, 1135−1154.

(25) Choi, J.-M.; Holehouse, A. S.; Pappu, R. V. Physical Principles Underlying the Complex Biology of Intracellular Phase Transitions. *Annu. Rev. Biophys.* **2020**, *49*, 107−133.

(26) Watanabe, H.; Ito, N.; Hu, C.-K. Phase Diagram and Universality of the Lennard-Jones Gas−Liquid System. *J. Chem. Phys.* **2012**, *136*, 204102.
(27) Goujon, F.; Ghoufi, A.; Malfreyt, P.; Tildesley, D. J. Can We Approach the Gas−Liquid Critical Point Using Slab Simulations of Two Coexisting Phases? *J. Chem. Phys.* **2016**, *145*, 124702.
(28) Silmore, K. S.; Howard, M. P.; Panagiotopoulos, A. Z. Vapour−Liquid Phase Equilibrium and Surface Tension of Fully Flexible Lennard-Jones Chains. *Mol. Phys.* **2017**, *115*, 320−327.
(29) Landau, L. On the Theory of Phase Transitions. *J. Exp. Theor. Phys.* **1937**, *7*, 19−32.
(30) Pelissetto, A.; Vicari, E. Critical Phenomena and Renormalization-Group Theory. *Phys. Rep.* **2002**, *368*, 549−727.
(31) Zollweg, J. A.; Mulholland, G. W. On the Law of the Rectilinear Diameter. *J. Chem. Phys.* **1972**, *57*, 1021−1025.
(32) Monahan, Z.; Ryan, V. H.; Janke, A. M.; Burke, K. A.; Rhoads, S. N.; Zerze, G. H.; O'Meally, R.; Dignon, G. L.; Conicella, A. E.; Zheng, W.; et al. Phosphorylation of the FUS Low-Complexity Domain Disrupts Phase Separation, Aggregation, and Toxicity. *EMBO J.* **2017**, *36*, 2951−2967.
(33) Pappu, R. V.; Wang, X.; Vitalis, A.; Crick, S. L. A Polymer Physics Perspective on Driving Forces and Mechanisms for Protein Aggregation. *Arch. Biochem. Biophys.* **2008**, *469*, 132−141.
(34) Zeng, X.; Pappu, R. V. Combined Theoretical and Computational Approach for Calculating Sequence-specific Phase Diagrams of Thermoresponsive Intrinsically Disordered Homopolypeptides. *Biophys. J.* **2020**, *118*, 304A.
(35) Zeng, X.; Holehouse, A. S.; Mittag, T.; Chilkoti, A.; Pappu, R. V. Connecting Coil-to-Globule Transitions to Full Phase Diagrams for Intrinsically Disordered Proteins. *BioRxiv* **2020**, DOI: 10.1101/2020.05.13.093351.
(36) Raos, G.; Allegra, G. Chain Collapse and Phase Separation in Poor-Solvent Polymer Solutions: A Unified Molecular Description. *J. Chem. Phys.* **1996**, *104*, 1626−1645.
(37) Crick, S. L.; Jayaraman, M.; Frieden, C.; Wetzel, R.; Pappu, R. V. Fluorescence Correlation Spectroscopy Shows That Monomeric Polyglutamine Molecules form Collapsed Structures in Aqueous Solutions. *Proc. Natl. Acad. Sci. U. S. A.* **2006**, *103*, 16764−16769.
(38) Vitalis, A.; Wang, X.; Pappu, R. V. Atomistic Simulations of the Effects of Polyglutamine Chain Length and Solvent Quality on Conformational Equilibria and Spontaneous Homodimerization. *J. Mol. Biol.* **2008**, *384*, 279−297.
(39) Milchev, A.; Paul, W.; Binder, K. Off-Lattice Monte Carlo Simulation of Dilute and Concentrated Polymer Solutions Under Theta Conditions. *J. Chem. Phys.* **1993**, *99*, 4786−4798.
(40) Lin, Y.-H.; Chan, H. S. Phase Separation and Single-Chain Compactness of Charged Disordered Proteins are Strongly Correlated. *Biophys. J.* **2017**, *112*, 2043−2046.
(41) Szleifer, I. A. New Mean-Field Theory for Dilute Polymer Solutions: Phase Diagram, Conformational Behavior and Interfacial Properties. *J. Chem. Phys.* **1990**, *92*, 6940−6952.
(42) Ganazzoli, F.; Raos, G.; Allegra, G. Polymer Association in Poor Solvents: From Monomolecular Micelles to Clusters of Chains and Phase Separation. *Macromol. Theory Simul.* **1999**, *8*, 65−84.
(43) Limbach, H. J.; Holm, C. Single-Chain Properties of Polyelectrolytes in Poor Solvent. *J. Phys. Chem. B* **2003**, *107*, 8041−8055.

https://dx.doi.org/10.1021/acs.jpclett.0c01222
J. Phys. Chem. Lett. 2020, 11, 4923−4929